Advanced Steel Construction – Vol. 22 No. 4 (2026) 368–382
DOI:10.18057/IJASC.2026.22.4.2

MECHANICAL BEHAVIOR AND YIELD-LINE-BASED DESIGN OF THROUGH-CORE BOLTED HSSC ANGLE JOINTS

Feng Zhu [1], Sen Li [1], Yun-Tao Shang [2], Han-Song Zhang [2], Jie Kong [2] and Le-Le Sun [2, *]

[1] *College of Civil Engineering and Architecture, Shandong Business Institute, Yantai, Shandong Province 264670, China*
[2] *Yantai Research Institute, Harbin Engineering University, Yantai, Shandong Province 264006, China*
* *(Corresponding author: E-mail: lelesun117@hrbeu.edu.cn)*

A B S T R A C T

Combined bolted angle beam to column joint had the advantages of high bearing capacity and considerable deformation capacity, which are desirable characteristics for semi-rigid connections considered in earthquake-resistant frame structures. This paper focuses on the fundamental bending performance and design of a novel connection type that using through-core bolts to connect the angle and hollow square section column (HSSC). The bending performance was simulated using the verified finite element model (FEM) by means of monotonic loading, and the parametric analysis included angle flange thickness, angle steel strength, bolt vertical distance, stiffening rib position, thickness, shape, and number and double web angles. The results showed that angle flange thickness, steel strength, and bolt vertical distance had significant impact on bearing capacity of joints and the parameter of stiffening rib had little effect on initial stiffness. For unstiffened angle joints, the pattern of yield line was three straight lines located at the root of angle flange, angle web, and throughout bolt holes, respectively. It can be changed to two circular arc curves by setting stiffening ribs, which increased the bearing capacity o f joints obviously. The web angle only formed yield line in tension zone and the pattern was the same as top angle. Three types of design method were proposed for unstiffened angle, stiffened angle, and web angle joints, respectively, by referring to the yield line theory given in Eurocode 3 and P398. Compared with results obtained from FEM, the calculated values were highly consistent with, demonstrating the reliability of the formula.

A R T I C L E H I S T O R Y

Received:	21 August 2025
Revised:	3 January 2026
Accepted:	4 January 2026

K E Y W O R D S

Angle connection;
Beam-column joint;
Numerical simulation;
Bending performance;
Design method

1. Introduction

In frame structures, beam-column joints were conventionally designed as rigid connections, wherein the beam and column members were welded to ensure sufficient structural strength. However, brittle fractures at the weld interfaces were frequently identified as a predominant failure mode. This limitation was notably exemplified by the 1994 Northridge earthquake in the United States [1] and the 1995 Hanshin earthquake in Japan [2], during which the inter-story drift angles were observed to exceed ductility limits, thereby inducing complete fracture propagation across welded zones and ultimately resulting in catastrophic structural failures. To overcome these limitations, researchers suggested using semi-rigid joints with high strength bolts, since these connections could satisfy both the strength and deformation requirements [3,4]. The behavior of semi-rigid joints was studied using moment-rotation (*M-θ*) curves [5], where two main properties moment resistance and rotational stiffness were measured. Fig. 1 showed *M-θ* curves for different types of semi-rigid joints [6], among which the top and seat angles connection was commonly used in earthquake-prone areas owing to its heavy ultimate moment and large deformation [7,8].

Davor Skejic et al. [9] conducted tensile and bending tests on stiffened angle connections, through which the yield lines of stiffened angles were identified. Based on the results giving a more precise assessment than Eurocode 3 [10]. Reinosa et al. [11] performed tensile tests on five sets of stiffened angle connection based on the tests conducted by Skejic [12] and established a simplified finite element model (FEM). Based on the numerical analysis, proposed an analytical method to determine the initial tensile stiffness of the joints. Movaghati et al. [13] investigated the effect of angle deformation on the nonlinear behavior and hysteresis behavior of beam to column connections by performing monotonic and cyclic loading tests. Wang et al. evaluated the bending performance of beam to H-column major-axis [14] and minor-axis [15] connections, along with the effect of bolt patterns on failure mode [16]. Zhang et al. [17] conducted monotonic tensile tests on stiffened angle to examine the impact parameters such as stiffening rib thickness, bolt arrangement, and bolt diameter on tensile strength, giving a mechanical model describing the load-displacement behavior of stiffened angle joints. Meng et al. [18] proposed an enhanced top and seat angles joints in order to address weak robustness under progressive collapse scenarios by incorporating four bent angles within the beam flange, and the efficacy of the design was confirmed through FEM.

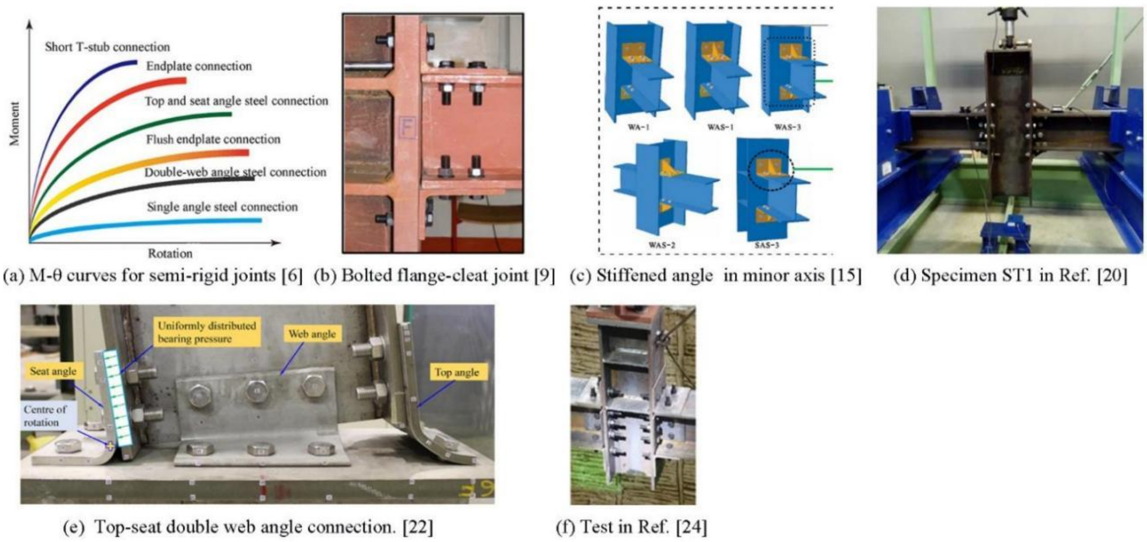

(a) M-θ curves for semi-rigid joints [6] (b) Bolted flange-cleat joint [9] (c) Stiffened angle in minor axis [15] (d) Specimen ST1 in Ref. [20]
(e) Top-seat double web angle connection. [22] (f) Test in Ref. [24]

Fig. 1 Several connected types in papers

Extensive research on double web angles connections was also conducted by various scholars. The *M-θ* behavior of double web angles joints were examined by Kong et al. [19], who developed improved equations for initial stiffness and ultimate moment capacity based on previous research. Similarly, Reinosa et al. [20] conducted eight tests on stiffened web angle in which the rotation of the beams was monitored, based on the results a calculation method for predicting rotational stiffness was proposed using the Eurocode 3 component method. Mohammad et al. separately investigated the *M-θ* behavior of both top and seat angles joints [21] and double web angles joints [22] fabricated from austenitic stainless steel, with test results confirming this material's exceptional ductility. Further investigation was carried out by Alhendi et al. [23], who numerically simulated the *M-θ* behavior of double web angles joints with varying steel grades. In a complementary study, the fire resistance of web angle joints was modeled by Cao et al. [24]. Results indicated that while thicker angles enhanced bearing capacity at ambient temperature, thinner angles demonstrated better performance under elevated temperatures.

However, the majority of existing research, including experimental validations, has focused on connections to H-shaped columns, as shown in Fig. 1(b)-(f). The behavior of semi-rigid angle connections to HSSCs, which offer distinct advantages in terms of bi-axial stiffness and architectural potential, remains significantly understudied, particularly for through-core bolted configurations. As a fundamental step towards understanding this novel joint, this study employs a numerically-driven approach. The primary objectives are: (1) to establish a reliable finite element modeling methodology for such connections; (2) to investigate the key parameters governing their monotonic bending behavior and failure mechanisms; and (3) to propose a yield-line-based analytical model for predicting their moment capacity. It is acknowledged that the proposed design methods are derived from numerical parametric studies, and their validation is based on verifying the FEM against established experimental benchmarks for analogous connection mechanics. Subsequent cyclic testing is required to fully assess seismic performance.

2. Research strategies

The mechanical performance of the joints was simulated using ABAQUS [25], which was recognized as widely used software for large-scale general-purpose FEM analysis. The simulations were conducted under monotonic static loading. This approach is adopted to establish a clear understanding of the joint's strength hierarchy, deformation capacity, and the formation of yield line mechanisms without the added complexity of load reversal. The derived moment capacity and stiffness parameters serve as direct inputs for nonlinear static analysis of frames and form the basis for planning future cyclic testing protocols.

2.1. Validations

2.1.1. General

To assess the accuracy of the FEMs applied in this paper, four specimens in Ref. [14] were selected to verify the accuracy of the material properties, boundary conditions and contact relationships in FEM, namely, specimen "SA-1", unstiffened angle connection, specimen "SAS-1", stiffened top angle connection, specimen "SAS-2", stiffened seat angle connection, and specimen "SAS-3", stiffened top and seat angles connection. The primary aim of this validation is not to directly validate the HSSC joint configuration itself, but to rigorously confirm that the developed FEM techniques, including material laws, contact interactions, bolt pretension, and element formulation, are capable of accurately capturing the complex mechanical behavior that is fundamental to all bolted angle connections. This established modeling framework is then applied with confidence to the parametric study of the through-core bolted HSSC joint, for which dedicated experimental data are currently scarce. In the validations, the cross-section of the H-column was HW250 × 255 × 14 × 14 and of the I-beam was HM194 × 150 × 6 × 9 mm, the angle was L140×90×8 mm, with a width of 150 mm. A total of 12 bolts with 10.9 grade M16 high strength were used to connect, and the preload was set to 100 kN. Detailed constructions were shown in Fig. 2.

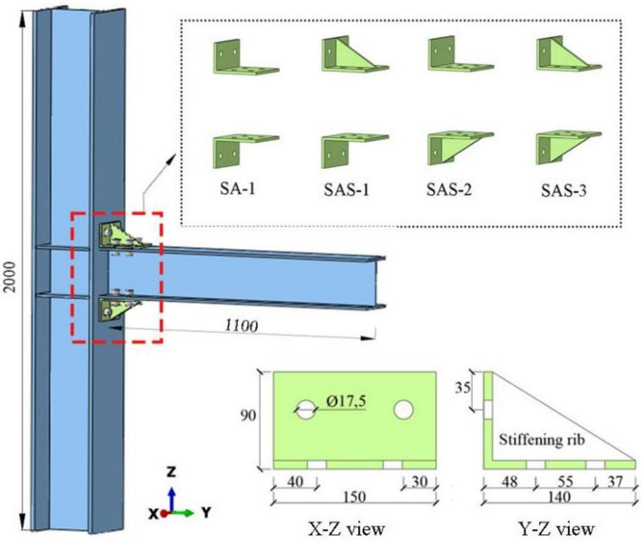

Fig. 2 Detailed constructions of test specimens in Ref. [14] (Unit: mm)

2.1.2. Finite element model

The FEM model had symmetry in geometric conditions, boundary conditions, and loading conditions, so the 1/2 model can be taken to save time and cost and improve calculation accuracy [26,27]. A simplified bilinear curves model was applied for stress-strain constitutive relationship of steel taken from Ref. [14], as shown in Table 1. All parts were modelled using 3-dimensional 8-node reduced integral units (C3D8R). A finer mesh size of 3 or 5 mm was used for the parts with large stress concentration and deformation, and a coarser mesh size of 15 or 20 mm was used where away from the core area.

The HSSC bottom surface was fully fixed in all degrees of freedom, simulating a rigid foundation. The top surface was constrained in all linear displacements but free to rotate, simulating a hinged support with the column inflection point assumed at mid-height. This boundary condition setup is representative of a typical beam-column sub-assembly test configuration and aims to isolate the joint behavior from global column bending, which is appropriate for a comparative parametric study focused on connection components. Surface-to-surface contact was defined between all interacting parts. The tangential behavior was modeled using the Coulomb friction model with a friction coefficient of 0.3. This value is specified for untreated steel surfaces in the Chinese design code GB50017-2017 [28] and aligns with common practice in analogous numerical studies of bolted connections. The "Hard" contact pressure-overclosure relationship was used for normal behavior, allowing for separation which is critical for capturing prying action. Bolt pretension was applied to the shank of each high-strength bolt to replicate the installed state. Geometric nonlinearity was included in the analysis step to capture large rotations and potential instability phenomena.

Table 1
Material properties of steel parts in Ref. [14] and mesh size

Steel parts	Thickness/mm	*E*/MPa	Yield strength/MPa	Ultimate strength/MPa	Elongation/%	Mesh size/mm
Column flange	14	204981	395	590	27.3	5/20
Column web	14	204981	395	590	27.3	5/20
Beam flange	9	207072	250	425	29.6	5/15
Beam web	6	207072	250	425	29.6	5/15
Angle	8	203500	245	360	30.2	5
Stiffening rib	8	199349	320	475	29.8	5
Welding plate	14	204922	245	415	28.3	10
Bolt	10.9 grade M16	206000	1020	1120	12.7	3

2.1.3. Results of validations

Fig. 3 showed the comparison of test and FEM results. For specimens SA-1 and SAS-2, the loading was expired due to the large deformation on top angle and the failure mode was the top angle tensile yielding. For specimens SAS-1 and SAS-3, the brittle fracture occurred at the welded connections between the stiffened top angle and stiffening rib which was not suitable to continue loading. It can be seen that the stiffened top angle flange significantly deformed and formed two arc curve yield lines, while the stiffened angle web formed one straight yield line paralleled to the web, as well as stiffened seat angle and stiffening rib showed compressive buckling. In summary, the results of failure mode FEM analysis were in good accordance with the test results.

The *M-θ* curve was defined as shown in Fig. 4(a), and the same approach was used in Refs. [29-31]. It can be seen that the stiffened angle joints fitted the test results, while the unstiffened joints were 14.3% lower than the tests result on yield strength. In summary, FEM curves basically coincided with the tests.

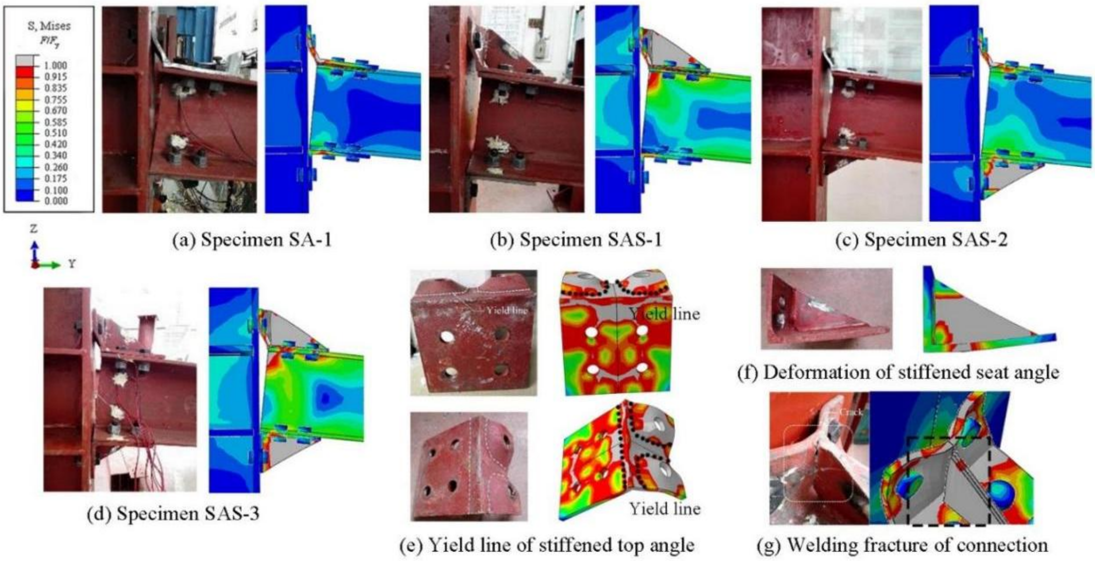

Fig. 3 Comparison of test and FEM results on deformation

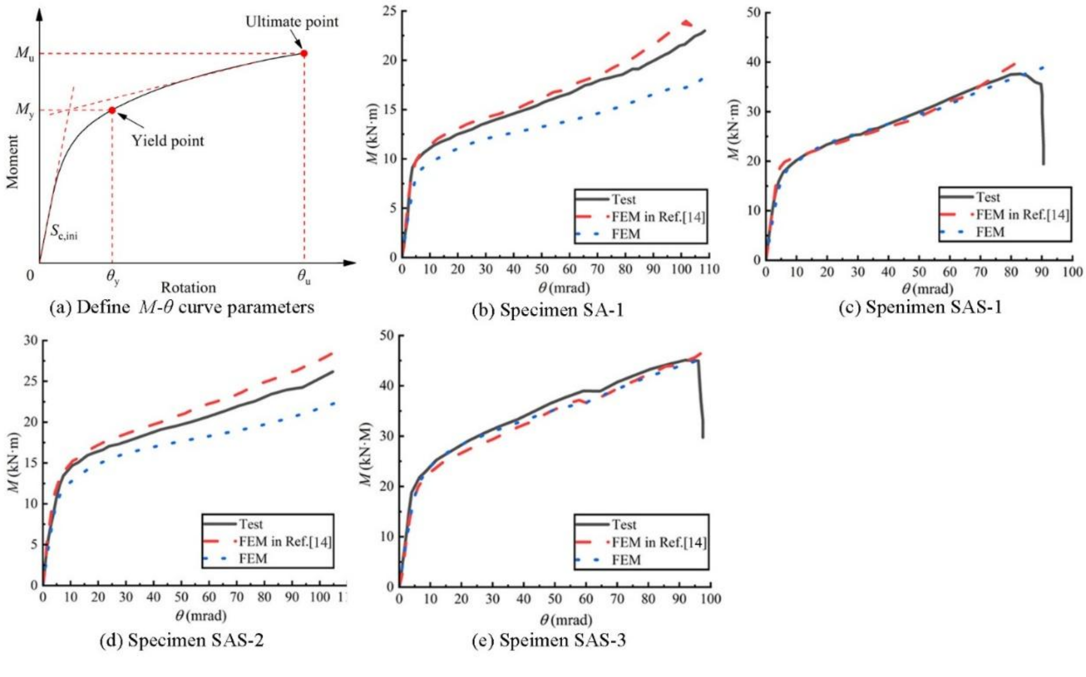

Fig. 4 Comparison of test and FEM *M-θ* curves

Table 2
Main results of test and FEM

Specimens	$S_{ini,test}$	$S_{ini,FEM}$	$S_{ini,test}/S_{ini,FEM}$	$M_{y,test}$	$M_{y,FEM}$	$M_{y,test}/M_{y,FEM}$	$M_{u,test}$	$M_{u,FEM}$	$M_{y,test}/M_{y,FEM}$
SA-1	2.899	2.389	1.213	11.37	9.94	1.144	22.87	18.18	1.258
SAS-1	4.866	3.605	1.349	19.09	19.11	0.992	35.45	34.62	1.024
SAS-2	3.096	2.248	1.377	15.03	13.26	1.133	26.54	21.91	1.211
SAS-3	5.030	4.192	1.199	23.63	23.68	0.997	45.70	44.78	1.021
Mean			1.284			1.066			1.128
Standard deviation			0.079			0.072			0.107

Note: S_{ini} (kN·m/mrad) denoted the initial stiffness; M_y (kN·m) and M_u (kN·m) denoted the yield moment and ultimate moment, respectively.

2.1.4. Sensitivity analysis of key modeling assumptions

Given the influence of modeling decisions on the simulated response of bolted connections, a focused sensitivity analysis was conducted on the unstiffened joint NT to assess the robustness of the primary findings. Three parameters were varied:

(1) Friction coefficient: Values of 0.2, 0.3, and 0.4 were modeled.

(2) Bolt pretension: Levels of 70 kN, 100 kN, and 130 kN were applied.

(3) Initial geometric imperfection: A local outward deviation of L/500 was introduced at the critical compressive zone of the seat angle web to trigger buckling modes.

The results, summarized in Table 3, indicate that while the absolute values of initial stiffness and yield moment showed some variation, the fundamental failure mechanism remained unchanged. Specifically, the formation of the three characteristic yield lines in the tension angle was consistently observed across all variations. The deformation patterns and the sequence of component yielding were not qualitatively altered. This demonstrates that the key conclusions regarding yield line patterns and the relative influence of geometric parameters are robust within a reasonable range of these modeling assumptions.

Table 3
Sensitivity analysis results for specimen NT

Model variant	Friction Coeff.	Bolt pretension (kN)	Imperfection	S_{ini} (kN·m/mrad)	M_y (kN·m)	Yield line pattern
Baseline NT	0.3	100	None	3.08	13.18	Three straight lines
Var. 1	0.2	100	None	2.95	12.85	Unchanged
Var. 2	0.4	100	None	3.18	13.42	Unchanged
Var. 3	0.3	70	None	2.92	12.91	Unchanged
Var. 4	0.3	130	None	3.21	13.52	Unchanged
Var. 5	0.3	100	*L*/500	3.05	12.95	Unchanged

2.2. Specimens design

The joint consisted of HSSC, HSS inner stiffener, I-steel beam, angles, stiffening ribs, high strength bolts, and through-core bolts. Among them, the cross-section of the HSSC was 200 × 200 × 10 mm, with a length of 1200 mm, the cross-section size of the HSS inner stiffener stiffener was 178 × 178 × 10 mm, with a length of 500 mm. The purpose of the HSS inner stiffener is to provide substantial lateral restraint to the HSSC wall, thereby mitigating excessive out-of-plane deformation under bolt prying forces [32,33]. This design detail aims to ensure that the failure mechanism is governed by yielding of the angles rather than localized distortion of the column face, creating a boundary condition for the angle that is more comparable to that provided by a stiffened flange of an H-column, as used in the validation models. The detailed construction was shown in Fig. 5 and material properties were used in Table 1.

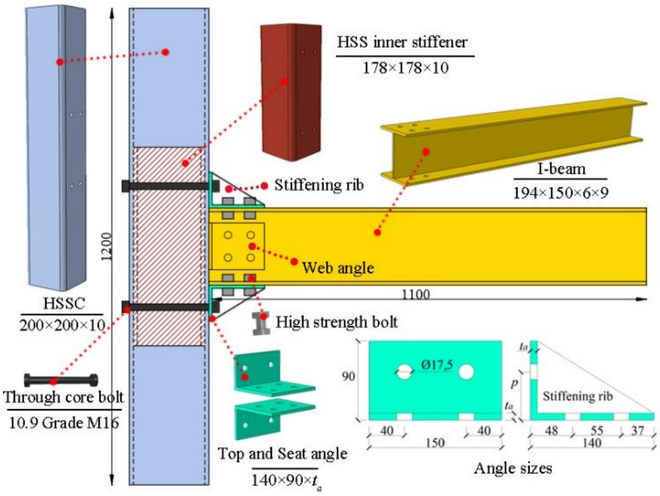

Fig. 5 Geometric construction of joints in this paper (Unit: mm)

In this paper, a total of 8 sets of FEMs were designed to study the bending performance, including angle thickness, angle steel strength, bolt vertical distance, stiffening rib position, stiffening rib shape, stiffening rib thickness, stiffening rib number, and double web angles, detailed parameters were shown in Table 4.

Table 4
FEM parameters

Specimens	Angle thickness/mm	Yield strength/MPa	*p*	Stiffening rib				Web angle	
				Position	Shape	Number	Thickness/mm	Angle thickness/mm	Rib thickness/mm
NT	**10**	245	55	null					
NT1	**8**	245	55	null					
NT2	**12**	245	55	null					
NT3	**14**	245	55	null					
NY1	10	**355**	55	null					
NY2	10	**390**	55	null					
NY3	10	**420**	55	null					
NY4	10	**460**	55	null					
NY5	10	**500**	55	null					
NP1	10	245	**45**	null					
NP2	10	245	**50**	null					
NP3	10	245	**60**	null					
NP4	10	245	**65**	null					

Specimens	Angle thickness/mm	Yield strength/MPa	*p*	Stiffening rib				Web angle	
				Position	Shape	Number	Thickness/mm	Angle thickness/mm	Rib thickness/mm
AR	10	245	55	**top-seat**	triangle	1	8		
AR1	10	245	55	**seat**	triangle	1	8		
AR2	10	245	55	**top**	triangle	1	8		
ARS1	10	245	55	top-seat	**rectangle**	1	8		
ARS2	10	245	55	top-seat	**pentagon**	1	8		
ARN1	10	245	55	top-seat	triangle	**2**	8		
ARN2	10	245	55	top-seat	triangle	**3**	8		
ART1	10	245	55	top-seat	triangle	1	**4**		
ART2	10	245	55	top-seat	triangle	1	**6**		
ART3	10	245	55	top-seat	triangle	1	**10**		
ART4	10	245	55	top-seat	triangle	1	**12**		
BR1	10	245	55	top-seat				**10**	
BR2	10	245	55	top-seat	triangle	1	8	**10**	**8**
BR3	10	245	55	top-seat				**10**	
BR4	10	245	55	top-seat	triangle	1	8	**10**	**8**

3. Parametric analysis

3.1. Parameters of angle

3.1.1. Effect of angle flange thickness

The effect of angle flange thickness on bending capacity was studied in this section and four FEMs were established to analyze. The thickness was ranged from 8 mm to 14 mm [34], and taken specimen VT (10 mm) as an example.

At the beginning of loading, the whole joint was in elastic stage. As the loading increased, the top angle flange in the tension zone gradually formed a gap with the column and detached. Continuing to the loading, the angle bent, firstly generating a yield line at the root of the angle. Simultaneously, a yield line was also generated at the root of the angle web, as show in Fig. 6. There was a clear concave circle around the bolt hole and a yield line was formed throughout it. The seat angle flange in the compression zone had no deformation but the web generated obvious bending deformation during the rotation of the beam. The stiffness of the column was much larger than that of the angle. Therefore, in the whole loading process, the column was always in the elastic working stage, and only the stress concentration occurred around the bolt hole.

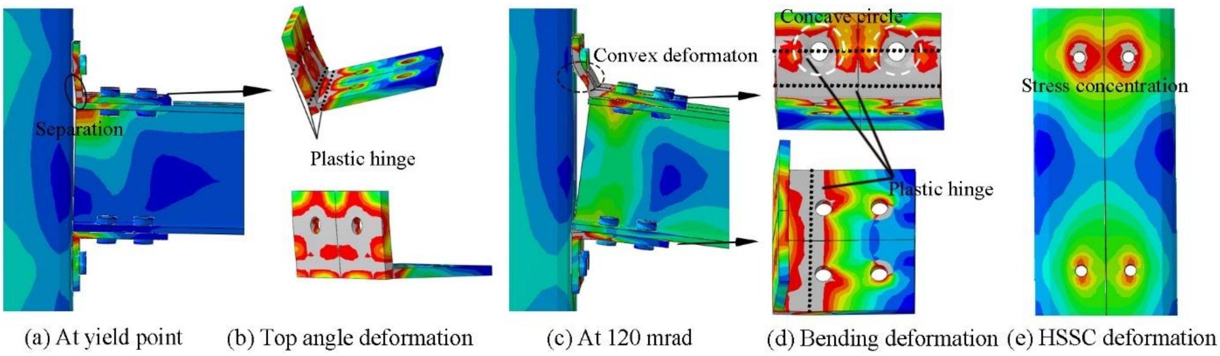

Fig. 6 Deformation of specimen VT as the loading continued

Fig. 7 and Table 5 shown the deformation, *M-θ* curves and main results for joints with different angle flange thickness. It can be seen that all the HSSCs were always in elastic working stage during the whole loading process at each joint. When the angle web was thinner, the beams hardly produced any deformation on specimens NT, NT1 and NT2. While the angle was thicker, the beam flanges near the rear of angle produced bending deformation as in specimens NT3 and NT4. Deformation at each joint was similar for both top angles in tension bending as well as seat angle in compression bending. Meanwhile, three yield lines were generated at the top angle and one yield line at the seat angle.

The initial stiffness, yield moment and ultimate moment of the joints were enhanced with the increase in the angle flange thickness. This was due to the fact that as the flange thickness increased, it improved the stiffness of the angle, which allowed the joint to withstand a greater loading at the same deformation.

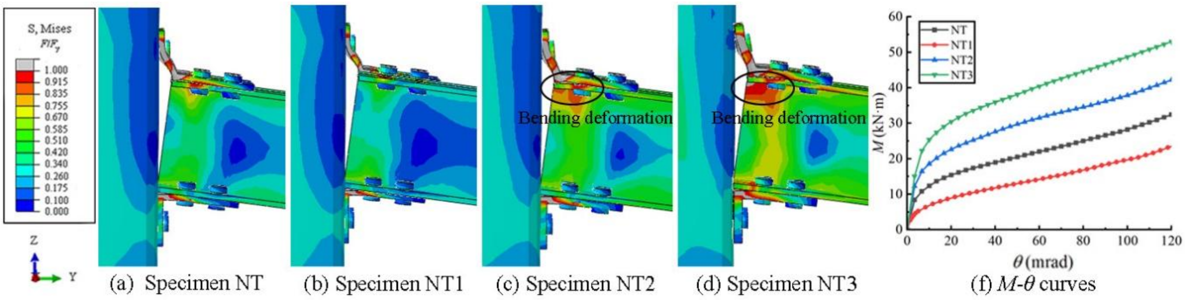

Fig. 7 Deformation of joints with different angle flange thicknesses

Table 5
Main results of the joints with different angle flange thicknesses

Specimens	Initial stiffness (kN·m/mrad)	Yield moment (kN·m)	Ultimate moment (kN·m)
NT	3.077	13.18	32.42
NT1	1.946	7.20	24.69
NT2	3.651	19.54	42.33
NT3	4.210	28.74	54.10

3.1.2. Effect of angle steel strength

The effect of angle steel strength on bearing capacity of joints was studied in this section and another five FEMs were established to analyse. The steels were taken as Table 1 Material properties of steel parts in Ref. [14] and mesh size and the nominal yield strength was taken as the yield strength according to 'GB/T19879-2023' [35]. The bilinear curve was shown in Fig. 8(a).

As can be seen from Fig. 8(b)-(f), the HSSCs and I-beams were hardly deformed and remained within the elastic state. The deformation in the joints were all taken by the angles and the angles produced similar deformation and plastic regions in each joint. Consistent with the section 3.1.1, the top angle flanges underwent bending deformation and gradually detached from the HSSC flange during the loading process. As loading continued, the aera of the angle plastic region increased, forming two yield lines at the root of the flange and web, respectively. The flange stretched outward, generating a concave circle along the bolt hole and a yield line throughout the bolt hole.

From Fig. 8(g) and Table 6, it can be seen that the increase in the angle strength had little effect on the initial stiffness of the joints, but improved the yield moment and ultimate moment clearly. When the angle yield strength was increased from 245 MPa to 355 MPa, the yield moment was increased by 46.13%. Continuing to increase the angle yield strength resulted in a small improvement, which was only when the yield strength increased from 355 MPa to 500 MPa that the yield moment increased by 38.42%.

As can be seen from Fig. 9, the increased of angle strength allowed the angle to withstand greater external loading within the same deformation. All top angles developed three plastic hinges including two hogging plastic hinges and one sagging plastic hinge.

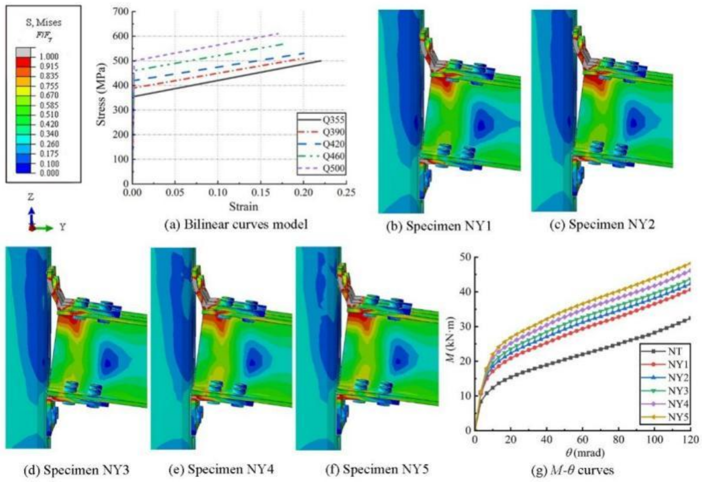

Fig. 8 Deformation of joints with different angle steel strengths

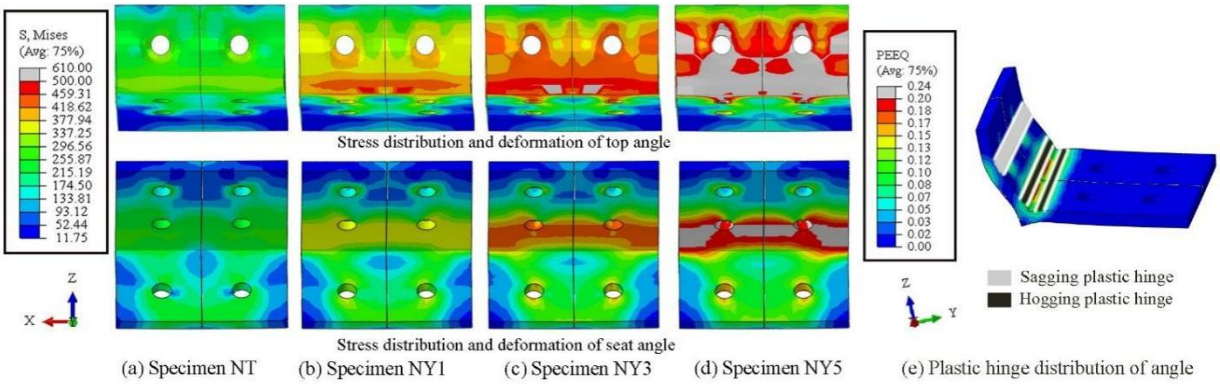

Fig. 9 Stress distribution and deformation of top and seat angles with different angle strengths

Table 6
Main results of joints with different angle strengths

Specimens	Yield moment (kN·m)	Increase over prior	Ultimate moment (kN·m)	Increase over prior
NT	13.18		32.42	
NY1	19.26	46.13%	40.65	25.38%
NY2	21.50	11.63%	42.03	3.39%
NY3	23.45	9.07%	43.74	4.06%
NY4	25.12	7.12%	46.12	5.44%
NY5	26.66	6.13%	48.20	4.51%

3.1.3. Effect of bolt vertical distance

In this section, another four FEMS were established to explore the effect of the bolt vertical distance p. The p was defined as the distance from the centre of angle flange bolt hole to the beam flange surface at intervals of 5 mm.

It can be seen from the Fig. 10(a)-(d) that the influence of the p on deformation and stress of the components of the joints except for the angles was small. Among all the joints, still only the angles underwent large deformation. The values of p had a greater effect on the stress distribution of angles. When the p was smaller, the plastic region was mainly concentrated in the lower flange. While the p was larger, the plastic region was divided into two portions, one was concentrated at the rear of the flange and the other was concentrated around the bolt holes, as shown in Fig. 10(e) and (f).

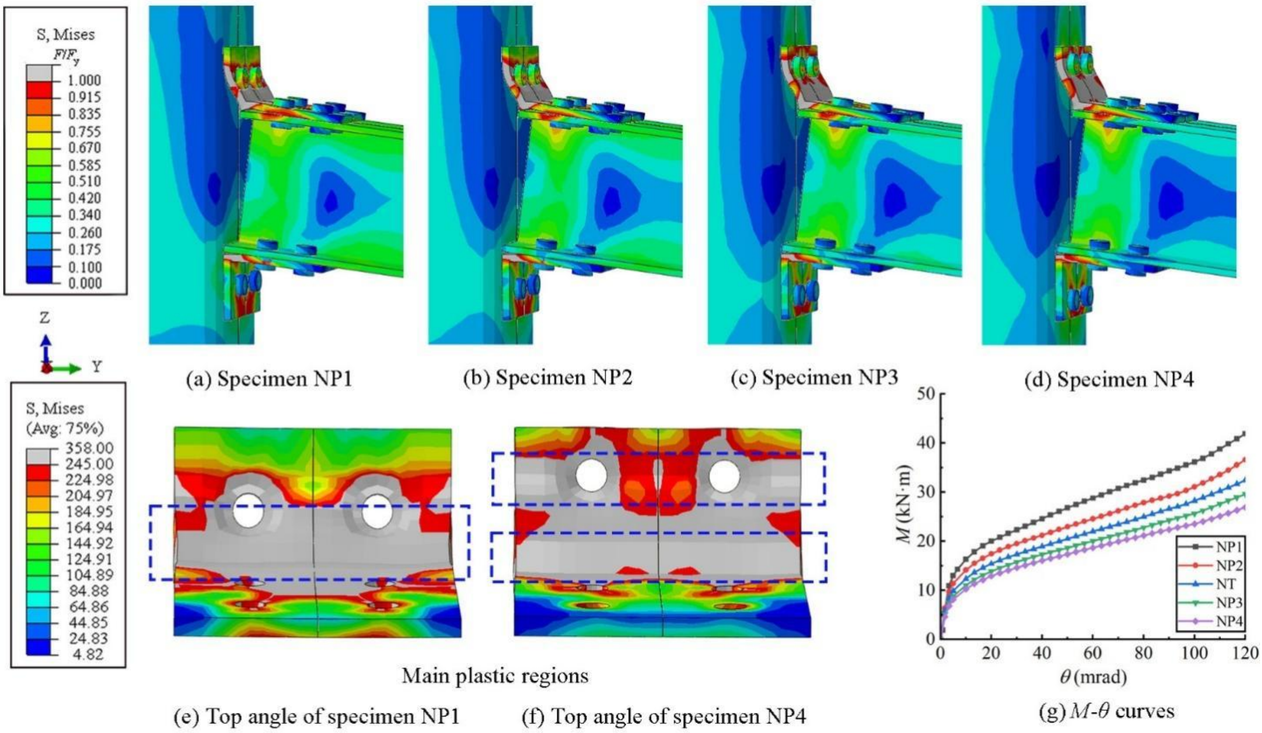

Fig. 10 Deformation of joints with different bolt vertical distance

The Fig. 10(g) and Table 7 illustrated the M-θ curves and main results of the joints. It can be seen that both the initial stiffness and ultimate moment decreased with the increased of the bolt vertical distance. When the p was larger, the deformation capacity of the angle was fully utilized, which was manifested in lower initial stiffness. With smaller p, the yield moment was elevated, attributed to the smaller distance between the two yield lines when the angle yielded.

Table 7
Main results of joints with different bolt vertical distance

Specimens	Initial stiffness (kN·m/mrad)	Yield moment (kN·m)	Ultimate moment (kN·m)
NP1	3.801	18.05	41.92
NP2	3.665	15.90	36.61
NT	3.077	13.18	32.42
NP3	2.891	12.55	29.59
NP4	2.751	11.79	26.89

3.2. Parameters of stiffening rib

3.2.1. Effect of stiffening rib position

The study on the position of stiffening rib included three specimens, namely, specimen AR, with both top and seat stiffening rib; specimen AR1, with seat stiffening rib; and specimen AR2, with top stiffening rib. The detailed construction of the joints was shown in Fig. 11(a) and (b).

From Fig. 11(c) and(d), the specimen AR1 with seat stiffening rib was top angle yield firstly and generated yield lines at the root of the flange and throughout bolt holes. At this time, the seat angle did not deform significantly while the seat stiffening rib formed a plastic region parallel to the hypotenuse and expanded inward. Until the loading ended, the top angle was subject to tensile bending and the seat angle and seat stiffening rib were compressive bending. Overall, the deformation of specimen AR1 was the same as specimen NT.

Unlike specimen AR1, the specimen AR2 was stiffening rib yield firstly. It can be seen from Fig. 11(c) and (d) that the top angle web did not deform significantly at this time, but the vertical middle of the flange deformed forward under the tension of the stiffening rib and separated from the column, forming two circular arc yield lines around the bolt holes. As loading continued, the top angle gradually separated from the column wall, with only the periphery of bolt holes remaining in contact with column under the bolt anchorage. The stiffening rib enhanced the stiffness of the angle, resulting a plastic region in the beam web. The seat angle deformed in the same as specimen NT.

Similarly, specimen AR was top stiffening rib yielded firstly. The deformation of the top angle was the same as that of specimen AR2 and the deformation of the seat angle and stiffening rib was the same as specimen AR1. A larger plastic hinge was formed at the beam web, as shown in Fig. 11(g) and (h).

The M-θ curves of four specimens apparently showed two groups and exhibited a large difference in both stiffness and ultimate moment. It can be found that the setting of the stiffening rib in the tension zone acted as an obvious role than that of in the compression zone, as shown in Table 8. That was due to the altered form of the yield line of the tensile angle. For the unstiffened top angle joints including specimens NT and AR1, the yield lines were along the width orientation, whereas the yield lines of stiffened joints including specimens AR and AR2 were two circular arcs around the bolt hole.

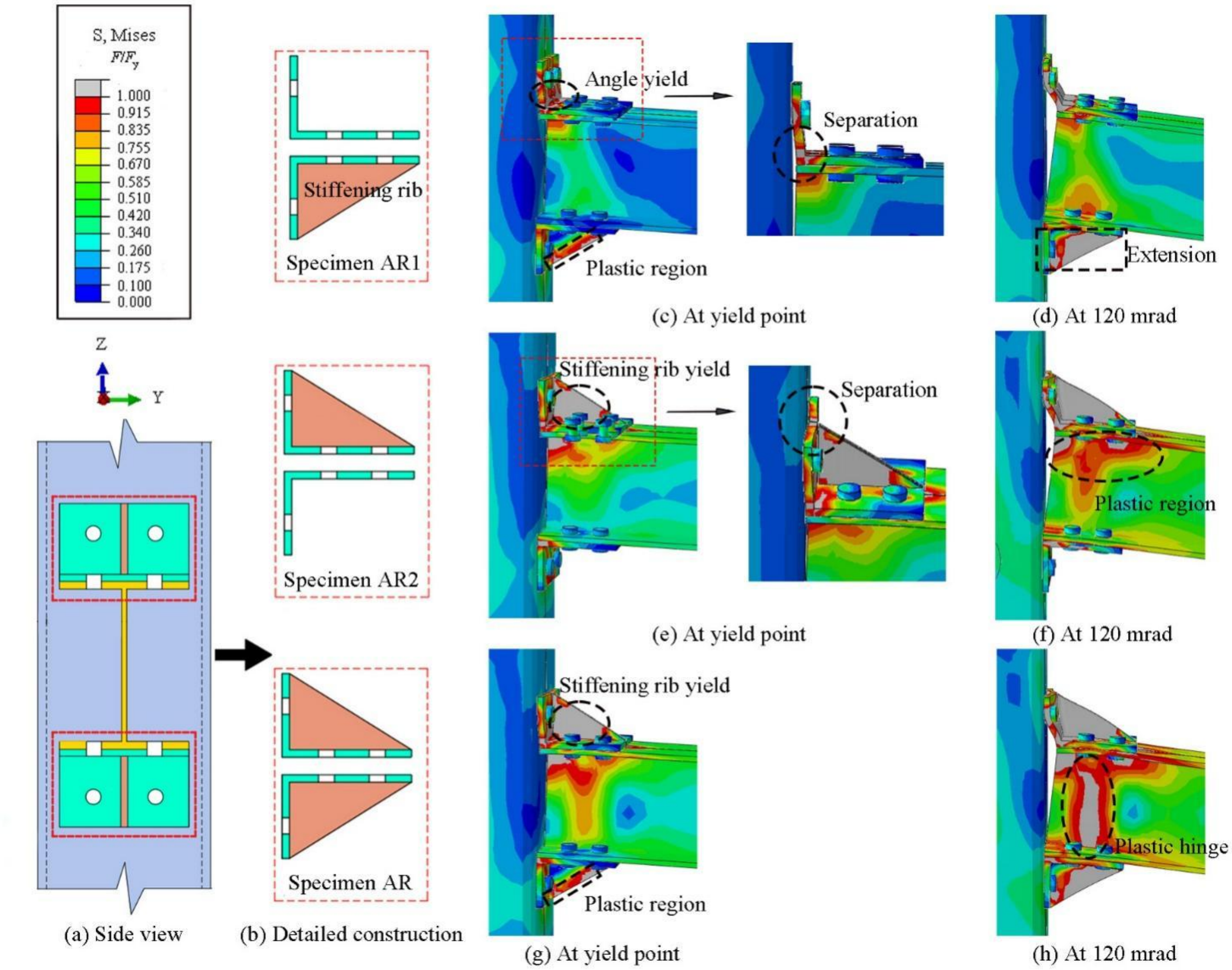

Fig. 11 Constructional details and deformation of joints with different stiffening rib position

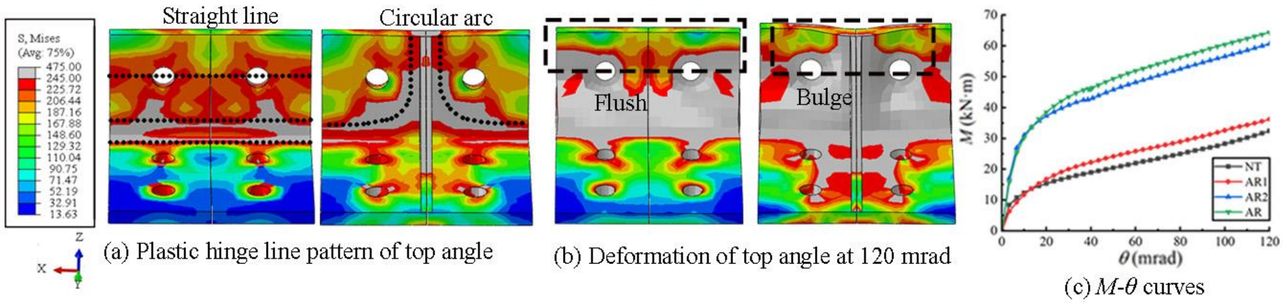

Fig. 12 Deformation of angles and M-θ curves

Table 8
Main results of joints with different stiffening rib position

Specimens	Initial stiffness (kN·m/mrad)	Yield moment (kN·m)	Ultimate moment (kN·m)
NT	3.077	13.18	32.42
AR1	2.895	15.14	36.23
AR2	4.874	35.59	60.69
AR	4.711	38.14	64.39

3.2.2. Effect of stiffening rib thickness

In this section, the effect of stiffening rib thickness on bearing capacity of the joints was investigated. Fig. 13 showed the deformation of the joints with different stiffening rib thickness at the yield point and 120 mrad, respectively. The specimen ART1 with thickness of 4 mm was top stiffening rib yielding completely first and the top angle did not deform significantly. The column and I-beam remained in elastic stage. Specimen ART2 with thickness of 6 mm was the same as stiffening rib yielding completely first. At this time the angle still had no significant deformation, only in the vertical middle of the flange there was a bending forward tendency. Specimen ART3 with thickness of 10 mm was the top angle and stiffening rib yielding almost simultaneously. A clear plastic region appeared at the end of the beam. Specimen ART4 with thickness of 12 mm was top angle yielding first with plastic region formed at the stiffening rib. The plastic region at the beam end was further enlarged. In all four specimens the angle yield pattern was two circular arcs around bolt holes.

As the loading continued, the angle, stiffening rib, and beam underwent bending deformation. It was found that the stiffness of the stiffening rib increased as the thickness growth, resulting in a decrease tendency of deformation, and the top angle web bent upward, creating a gap with the beam. Moreover, the yielding of beams increased significantly. Of 4 mm, the beam showed hardly any deformation, and of 10 and 12 mm, the beam generated a plastic hinge.

Fig. 14 showed the M-θ curves of the joints with different thicknesses of stiffening ribs. It can be seen that the thickness of the stiffening rib had little effect on the initial stiffness, but increased the yield moment, yield angle rotation and ultimate moment. This was due to the expansion of the angle yield region, which resulted in the translation of the yield line towards the vertical middle of the angle flange, increasing the effective length.

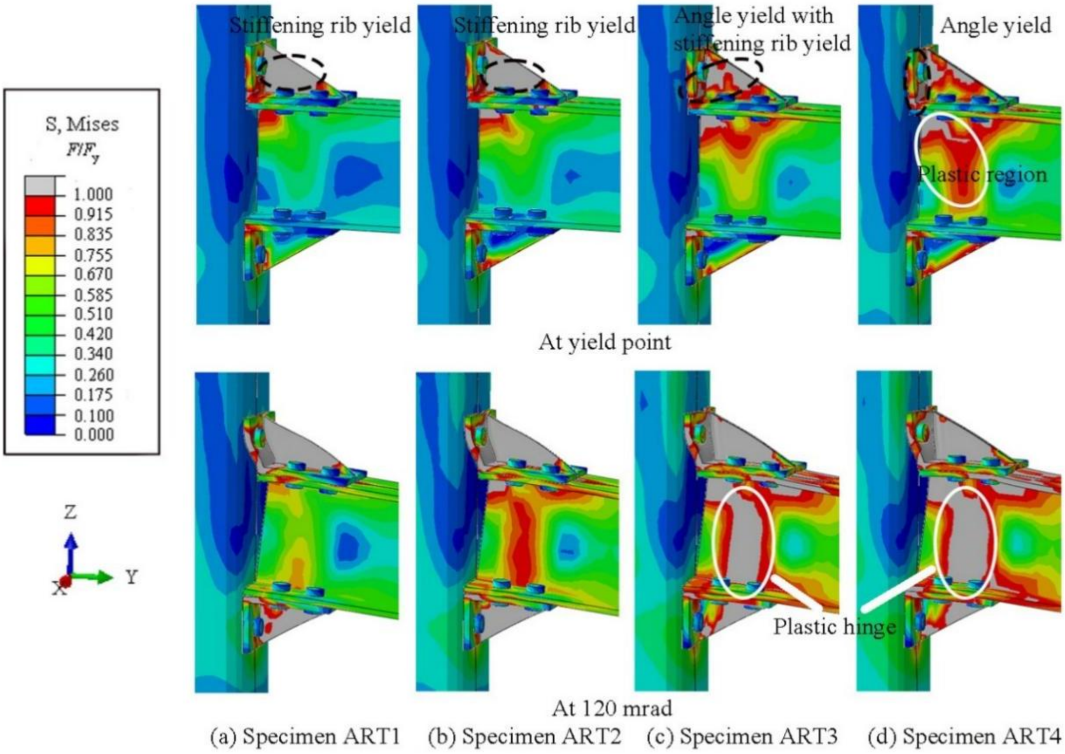

Fig. 13 Deformation of joints with different stiffening rib thicknesses

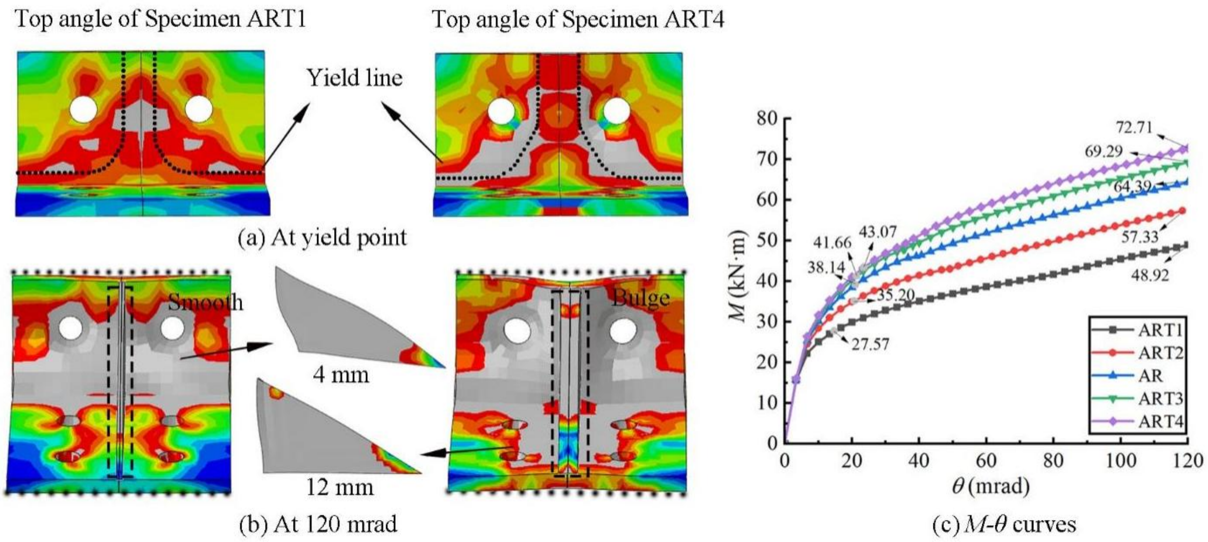

Fig. 14 Deformation of top angles and M-θ curves

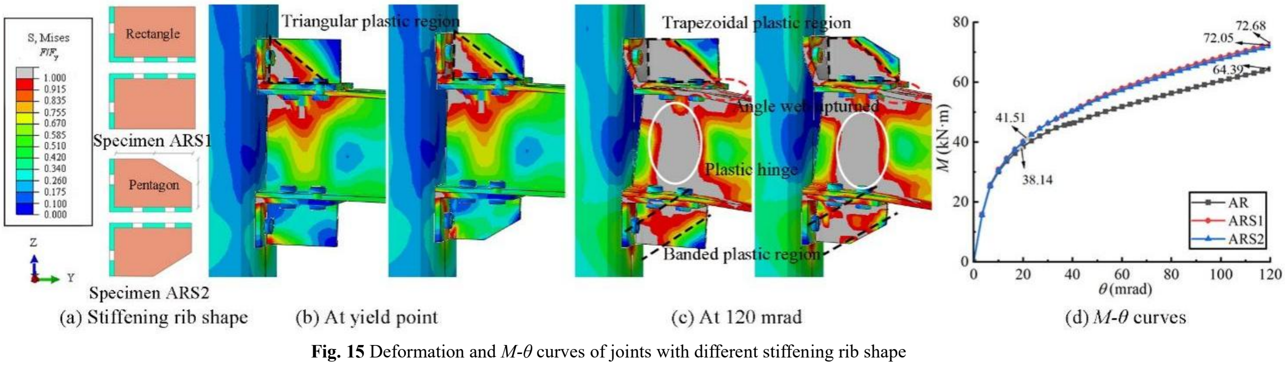

Fig. 15 Deformation and M-θ curves of joints with different stiffening rib shape

3.2.3. Effect of stiffening rib shape

In this section, the effect of stiffening rib shape was investigated, including specimen ARS1 with rectangular rib and specimen ARS2 with pentagonal rib, as shown in Fig. 15(a).

Similar to the specimen AR with triangular rib, the specimen ARS1 and ARS2 were top stiffening rib yielded before the angle. As the joints reached at the yield point, the top angle had the same deformation and the top stiffening rib showed a triangular yield region. The seat stiffening rib was almost in an elastic state.

As loading continued, the beam showed significant bending deformation and formed plastic hinges. At 120 mrad, compared to specimen AR, the stiffening rib of specimens ARS1 and ARS2 had less deformation and almost the same plastic region with a trapezium. The seat stiffening rib remained in its original shape and the plastic region was ribbon-like, as shown in Fig. 15(b) and (c).

There was no effect on the initial stiffness of joints by changing the stiffening rib shape. The M-θ curves of specimens ARS1 and ARS2 were shown in Fig. 15(d) almost coincided and revealed the same mechanical relationship. Moreover, the stress area of the stiffening ribs was increased, which led to an increase in both yield strength and ultimate moment.

3.2.4. Effect of stiffening rib number

In this section, two specimens were established to analyse the effect of the number of stiffening ribs, i.e., specimen ARN1 with two stiffening ribs arranged on each side of the angle and specimen ARN2 with three stiffening ribs arranged on each side and the middle of the angle, as shown in Fig. 16(a).

The specimen ARN1 was top angle yielding before other parts and the plastic region was mainly concentrated on the top angle when the joint reached at the yield point. Under the action of the stiffening rib, the flange and web of the angle bent along the vertical centreline and separated from the column and beam, respectively, meanwhile the stiffening rib bent inward. The seat angle and stiffening rib produced no deformation. When the angle yielded, the yield line pattern changed to a straight line through the bolt hole and a circular arc around the bolt hole.

The specimen ARN2 was beam yielding first and produced a plastic hinge, which was different from all the joints aforementioned. The top and seat angles and stiffening ribs did not develop any deformation, but formed different plastic regions respectively.

As the loading continued, the top angle flange of specimen ARN1 was bending forward on two sides, and the web was bending upward on two sides, characterized as high sides and low centre, while the top stiffening ribs were concave to the inside. The top angle flange of specimen ARN2 were bending forward in the middle and on both sides, with the shape of a wave, and the web were bending upward to different extents. The seat angle of specimens ARN1 and ARN2 were bending downward and the seat stiffening ribs of specimen ARN1 produced significant outward bending deformations than specimen ARN2. Compared to specimen ARN1, the specimen ARN2's beam produced larger bending deformation and plastic hinge.

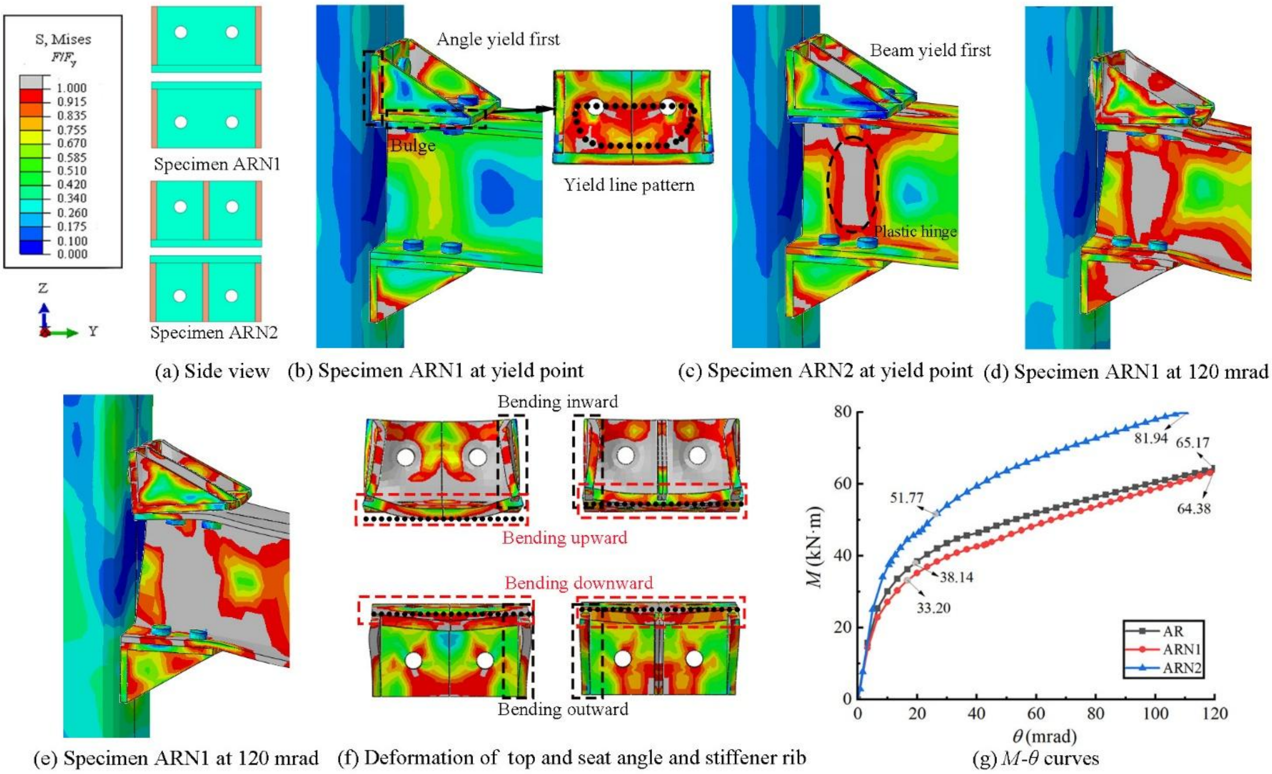

Fig. 16 Deformation and M-θ curves of joints with different stiffening rib number

3.3. Effect of double web angles

In this section, the effect of the double web angles on the bending performance of the joints was investigated. Four specimens were conducted with web angles or stiffened web angles, respectively. The web angle was the same size as the top and seat angles, and the detailed construction was shown in Fig. 17.

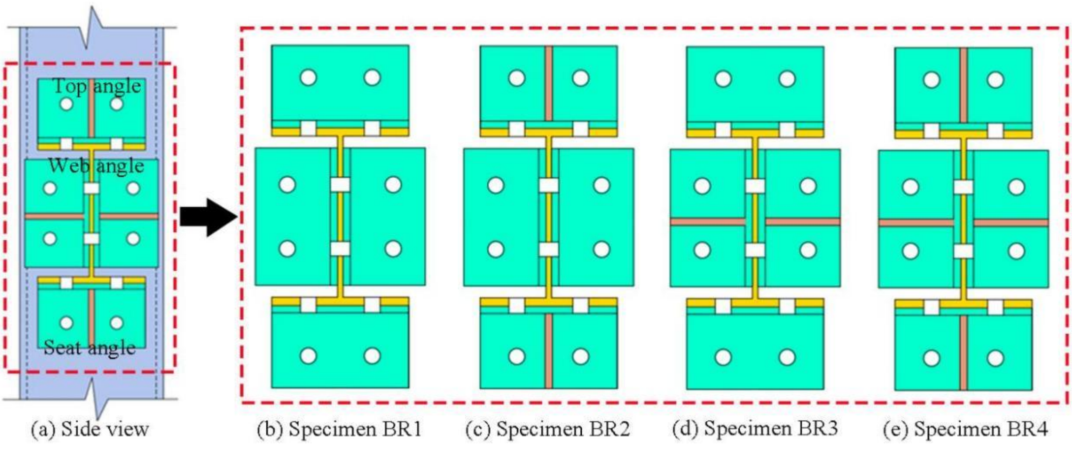

Fig. 17 Detailed constructions of double web angles joints

From Fig. 18, it can be seen that when the joints yielded, the columns and beams were still in the elastic stage. The force and deformation of the joints were mainly borne by the angles and stiffening ribs. For unstiffened web angle specimens BR1 and BR2 and the stiffened web angle specimens BR3 and BR4, the deformation and stress distribution of the top and seat angles were similar to those of without web angle joints, and the pattern of the yield lines was not changed. The web angle joints formed plastic hinges only in the tension zone of the flange, and the difference was in the form of the yield line. For unstiffened web angle joint specimen BR1, the yield line was linear, while a circular arc for the stiffened web angle.

Fig. 19 showed the joints at 120 mrad. The flange of the web angle in the tension zone was obviously detached from the column, while the flange in the compression zone was adhered to the column with the web angle twisted. Due to the top and seat stiffening rib, the deformation and plastic region of the web stiffening ribs of specimen BR4 were smaller than that of specimen BR2. However, the beams were on the contrary, the beam flange of specimen BR1 was flat with almost no deformation, the specimens BR2 and BR3 produced bending deformation, and the plastic hinge region of specimen BR3 was larger, and even local buckling occurred at specimen BR4.

Fig. 20 and Table 9 showed the M-θ curves and main results of the web angle joints. It can be seen that the web angle, by assuming the forces and deformations, resulted in an increase in both the yield strength and ultimate moment of the joints.

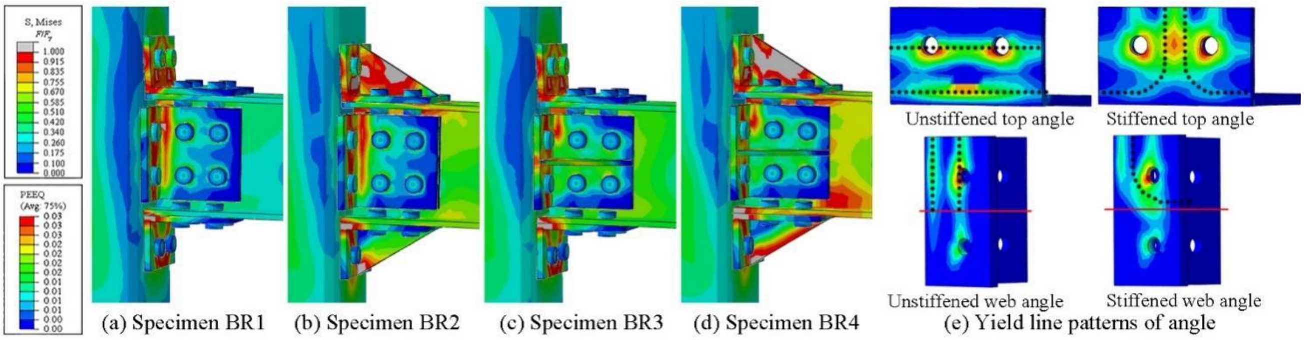

Fig. 18 Deformation of joints at yield point with double web angles

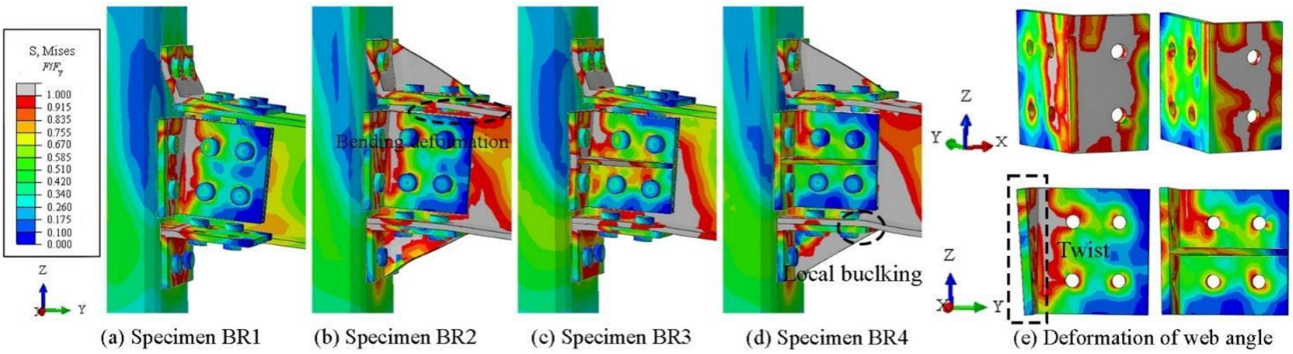

Fig. 19 Deformation of joints at 120 mrad with double web angles

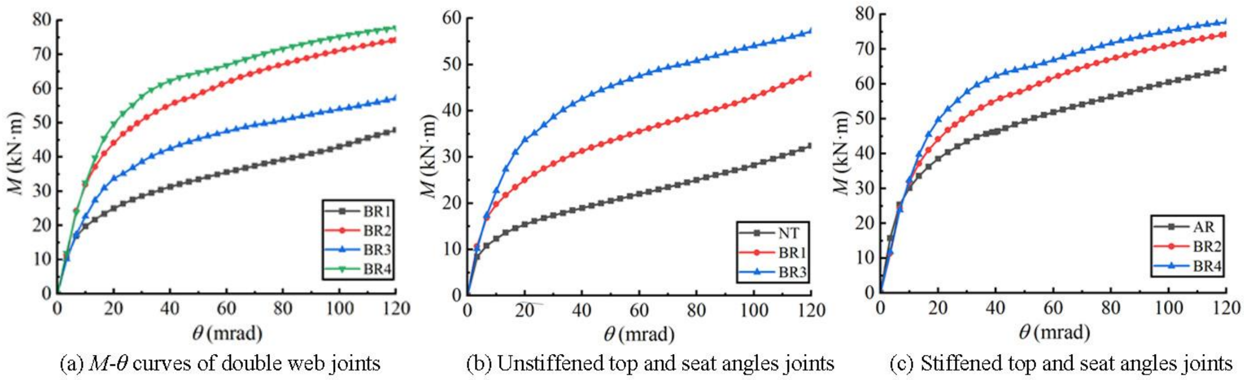

Fig. 20 M-θ curves of joints with double web angles joints

Table 9
Main results of joints with double web angles joints

Specimens	Initial stiffness (kN·m/mrad)	Yield moment (kN·m)	Ultimate moment (kN·m)
BR1	3.255	24.08	47.85
BR2	4.304	48.53	74.03
BR3	3.171	35.84	57.18
BR4	4.395	59.49	77.83

4. Calculation of bending capacity of angle joints

The mechanical performance of combined bolted angle beam to HSSC connection joint under monotonic loading was revealed by means of FEM in terms of stress distribution, deformation and bearing capacity. In order to be applied in the design work, the calculation method was proposed in this section. The yield line theory was widely used to calculate the bending capacity, which was recommended by Eurocode 3 and P398 [36].

The yield line models and the accompanying design equations proposed in the following subsections were developed and validated within the parameter ranges investigated in the numerical parametric study. The applicability of this method is therefore bounded by the following limits, which define the database from which it was derived:

(1) Angle geometry: Leg length of 140 mm × 90 mm; thickness t_a = 8mm-14 mm.

(2) Bolt layout: Two bolts in a vertical line in the outstanding leg; bolt gauge g = 70 mm; vertical distance from beam flange p = 45mm-65 mm.

(3) Stiffener geometry: Triangular, rectangular, or pentagonal shape attached to the angle leg; stiffener thickness t_s = 4mm-12 mm.

(4) Material: Structural steel with nominal yield strength f_y = 245MPa-500 MPa, exhibiting ductile behavior.

The equations calculate the characteristic bending resistance M_{Rk} of the joint components. For design purposes, this resistance must be divided by the appropriate partial safety factor γ_{M2} as stipulated by Eurocode 3-1-8 [37] to obtain the design bending resistance M_{Rd}.

4.1. Unstiffened top and seat angles joints

For unstiffened top and seat angles joints, two yield lines were generated when the angle yielded. One yield line was at the root of the flange and the other yield line passed through the bolt hole. The tensile capacity of the angle flange yielded can be calculated using follows:

$$F_{T1,Rd}=\frac{2M_{pl1,Rd}}{m} \tag{1}$$

$$M_{pl1,Rd}=0.25\sum l_{eff,un}t_a^2 f_y \tag{2}$$

$$m=p-t_a \tag{3}$$

$$\sum l_{eff,ns}=l_{eff,1}+l_{eff,2}=2t_w-2d_0 \tag{4}$$

where, t_a was the thickness of angle flange and web, t_w was the width of angle, f_y was the angle steel yield strength, d_0 was the diameter of bolt hole, *and* m was the distance between two yield lines, as shown in Fig. 21. $M_{pl1,Rd}$ was each yield line by the external moment and $\sum l_{eff,un}$ was the sum of effective length of unstiffened angle yield lines.

Therefore, the characteristic bending resistance of an unstiffened angle joint component can be calculated as:

$$M_{T1,Rk}=F_{T1,Rk}H_1 \qquad M_{T1,Rd}=M_{T1,Rk}/\gamma_{M2} \tag{5}$$

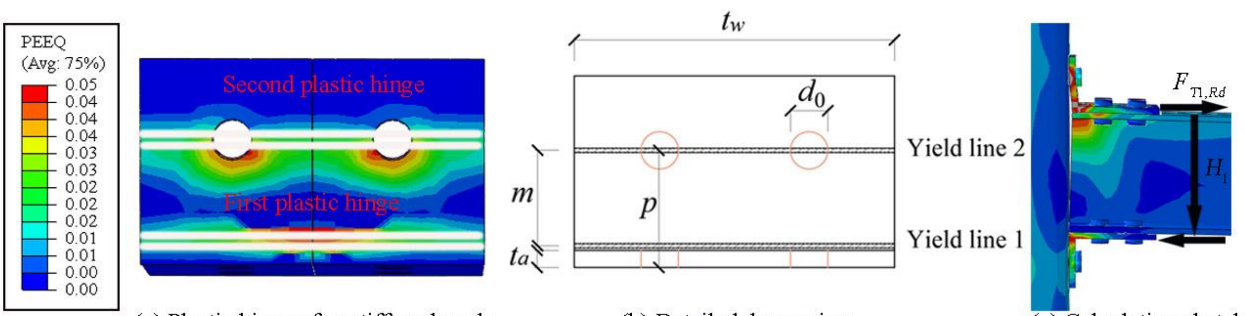

(a) Plastic hinge of unstiffened angle (b) Detailed demension (c) Calculation sketch

Fig. 21 Simplified diagrams for calculating unstiffened angle yield capacity

Table 10
Comparison of calculation and FEM of unstiffened angle joints

Specimens	t_a	f_y	$\sum l_{eff}$	p	m	M_{cal}	M_{FEM}	M_{cal}/M_{FEM}
NT	10	245	265	55	45	15.44	13.18	1.171
NT1	8	245	265	55	47	9.28	7.2	1.289
NT2	12	245	265	55	43	23.70	19.54	1.213
NT3	14	245	265	55	41	34.45	28.74	1.199
NY1	10	355	265	55	45	22.37	19.26	1.161
NY2	10	390	265	55	45	24.57	21.5	1.143
NY3	10	420	265	55	45	26.46	23.45	1.128
NY4	10	460	265	55	45	28.99	25.12	1.154
NY5	10	500	265	55	45	31.51	26.66	1.182
NP1	10	245	265	45	35	19.85	18.05	1.110
NP2	10	245	265	50	40	17.37	15.9	1.092
NP3	10	245	265	60	50	13.89	12.55	1.107
NP4	10	245	265	65	55	12.63	11.79	1.071
Mean								1.155
Standard deviation								0.056

The predictive capability of Eqs. (1)-(5) is evaluated by direct comparison with the FEM yield moments M_{FEM} from the parametric study, as summarized in Table 10. No empirical calibration factors are applied to the FEM results. The calculated yield moments M_{cal} show a consistent, slight overestimation compared to the FEM benchmarks. The mean ratio M_{cal}/M_{FEM} for all 13 unstiffened specimens is 1.155 with a standard deviation of 0.057, indicating that the proposed yield line model predicts, on average, a yield strength approximately 15.5% higher than the finite element simulation.

This conservative bias is rationally explained by the idealizations inherent in the yield line theory. The analytical model assumes the formation of discrete, perfect plastic hinges, whereas the FEM captures a more realistic gradual spread of plasticity, stress concentrations around bolt holes, and detailed deformation compatibility. The close agreement across a wide range of independent parameters demonstrates the robustness and predictive validity of the formulation within the investigated parameter space. The consistent overestimation renders the method inherently conservative for strength prediction.

4.2. Stiffened top and seat angles joints

For stiffened top and seat angles joints, the pattern of yield lines was two circular arcs as the stiffened angle yielded. The tensile capacity of the stiffened angle flange yielded can be calculated using follows:

$$F_{T2,Rd}=\frac{2M_{pl2,Rd}}{m_1} \tag{6}$$

$$M_{pl2,Rd}=0.25\sum l_{eff,st}t_a^2 f_y \tag{7}$$

$$m_1=p-t_a \tag{8}$$

$$m_2=0.25g+0.6t_s \tag{9}$$

$$\sum l_{eff,st}=(6m_2-0.625n_2+n_1)*2 \tag{10}$$

for specimen ARN1:

$$\sum l_{eff,st}=(6n_2-0.625m_2)*2+g-d_0 \tag{11}$$

where, n_1 and n_2 were the distance from the bolt hole to the free edge of the angle, respectively. m_1 and m_2 were the distance from the bolt hole to the yield line, respectively. t_s was the thickness of stiffening rib, g was the gauge of the bolt, as shown in Fig. 22. $M_{pl2,Rd}$ was each yield line by the external moment and $\sum l_{eff,st}$ was the sum of effective length of stiffened angle yield lines.

Therefore, the yield bending capacity of stiffened angle joints can be calculated using the following formula:

$$M_{\mathrm{T2,Rk}} = F_{\mathrm{T2,Rk}} H_1 \qquad (12)$$
$$M_{\mathrm{T2,Rd}} = M_{\mathrm{T2,Rk}} / \gamma_{\mathrm{M2}}$$

The calculations given by Eqs. (6)-(12) were shown in Table 11 and compared with the results obtained by FEMs in Section 3. It was clear that the majority of calculated values are 10%-20% lower than the FEM results. This indicates that the proposed model for stiffened angles provides a built-in safety margin for design within the studied parameter range.

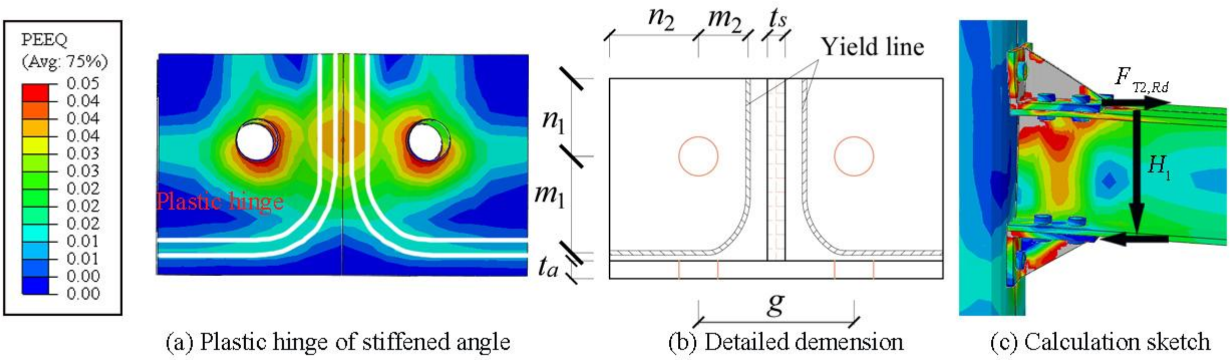

Fig. 22 Simplified diagrams for calculating stiffened angle yield capacity

Table 11
Comparison of calculation and FEM of stiffened angle joints

Specimens	n_1	n_2	m_1	m_2	ts	g	$l_{eff,st}$	M_{cal}	M_{FEM}	M_{cal}/M_{FEM}
AR	35	40	45	22.3	8	70	287.6	33.51	38.14	0.879
ART1	35	40	45	19.9	4	70	258.8	30.15	27.57	1.094
ART2	35	40	45	21.1	6	70	273.2	31.83	35.2	0.904
ART3	35	40	45	23.5	10	70	302	35.19	41.66	0.845
ART4	35	40	45	24.7	12	70	316.4	36.86	43.07	0.856
ARS1	35	40	45	22.3	8	70	287.6	33.51	41.51	0.807
ARS2	35	40	45	22.3	8	70	287.6	33.51	41.51	0.807
ARN1	35	35	45	24.8	8	70	288.8	33.65	33.20	1.014
ARN2								beam yield	51.77	
Mean										0.901
Standard deviation										0.096

4.3. Double web angles joints

For double web angles joints, the calculation of the bending capacity can be carried out directly on the basis of the unstiffened top and seat angles joints or stiffened top and seat angles joints. The pattern of the web angle plastic hinge was the same as that of the top and seat angles, with the difference that the plastic hinge was generated only in the tension zone. The tensile capacity of the web angle flange yielded can be calculated using follows:

$$F_{T3,Rd} = \frac{2M_{pl3,Rd}}{m_x} \qquad (13)$$

$$M_{pl3,Rd} = 0.25 \sum l_{eff,\mathrm{web}} t_a^2 f_y \qquad (14)$$

$$m_x = p - t_a \qquad (15)$$

$$m = 0.25g + 0.6t_s \qquad (16)$$

$$\sum l_{eff,\mathrm{web}} = \begin{cases} \sum l_{eff1,\mathrm{web}} = t_w - d_0 & \text{unstiffened web angle} \\ \sum l_{eff2,\mathrm{web}} = 6m - 0.625e + e_x & \text{stiffened web angle} \end{cases} \qquad (17)$$

where, $M_{pl3,Rd}$ was each yield line by the external moment and $\sum l_{eff,web}$ was the sum of effective length of double web angles yield lines. Other parameters were shown in Fig. 23.

Therefore, the yield bending capacity of web angle joints can be calculated using the following formula:

$$M_{\mathrm{T3,Rk}} = F_{\mathrm{T(1,2),Rk}} H_1 + 2F_{\mathrm{T3,Rk}} H_2 \qquad (18)$$
$$M_{\mathrm{T3,Rd}} = M_{\mathrm{T3,Rk}} / \gamma_{\mathrm{M2}}$$

where, $F_{T(1,2),Rd}$ indicated that the unstiffened top and seat angles joints were taken as $F_{T1,Rd}$ while the stiffened top and seat angles joints were taken as $F_{T2,Rd}$. H_1 and H_2 were the distance between the rotation centre of the tension zone and the compression zone of top angle and web angle, respectively.

The calculations given by Eqs. (13)-(18) were shown in Table 12 and compared with the results obtained by FEMs in Section 3. It was observed that the majority of computational errors fall within the range of 10%. In conclusion, these equations were suitable for calculating the bending capacity of double web angles joints.

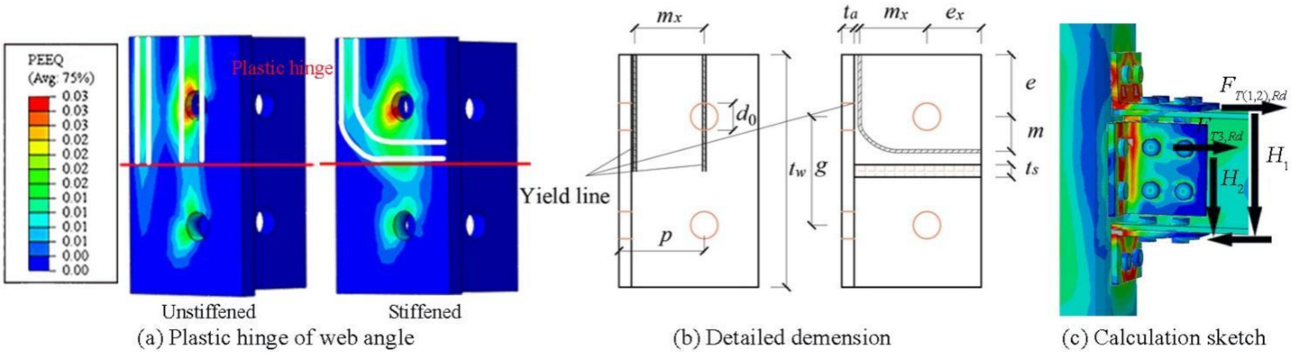

Fig. 23 Simplified diagrams for calculating double web angles yield capacity

Table 12
Comparison of calculation and FEM of double web angles joints

Specimens	e_x	e	m_X	m	ts	g	$l_{eff,web}$	M_{cal}	M_{FEM}	M_{cal}/M_{FEM}
BR1	35	40	45			70	132.5	25.68	24.08	1.066
BR2	35	40	45			70	132.5	43.75	48.53	0.902
BR3	35	40	45	22.3	8	70	143.8	37.67	35.84	1.051
BR4	35	40	45	22.3	8	70	143.8	55.74	59.49	0.937
Mean										0.989
Standard deviation										0.071

5. Conclusions

In this paper, the mechanical performance of the combined bolted angle HSSC to I-beam connection joints was carried out by the verified FEM, and the impact of parameters on the bending capacity of the angle was investigated. The yield capacity had been calculated by applying the yield line theory. Based on the research in this paper, the following conclusions can be drawn:

(1) The unstiffened top angle generated three yield lines in tension bending, all of which were straight, located at the root of the web, at the root of the flange and through the bolt holes, respectively. The unstiffened seat angle generated only one yield line at the rear of web.

(2) Increasing the thickness and strength of the angle, as well as decreasing the bolt vertical distance can improve the bearing capacity of the joints, with changing the flange thickness had the most significant effect. Adjusting the flange thickness and bolt vertical distance can change the initial stiffness of the joints, attributed to changing the angle cross sectional shape.

(3) The initial stiffness and bearing capacity of the joints can be significantly increased by setting stiffening ribs due to the change in the yield line pattern of the angle, which effectively increased the effective length of the yield line and generated a plastic hinge in the beam. Compared to triangular stiffeners, rectangular and pentagonal ribs increased the bearing capacity by enlarging the force region.

(4) The thickness of the stiffening ribs had a great influence on the deformation of the joints. The deformation of 4 mm stiffening ribs was large while the beam did not deform and the deformation of 12 mm stiffening ribs was small but the beam generated plastic hinge. Setting the stiffening ribs on angle sides reduced the bearing capacity, and setting three stiffening ribs caused the beam to yield before the angle.

(5) For web angle joints, the forces and deformations of top and seat angles were the same as in joints without web angles. The web angle underwent torsional deformation and the yield line pattern was the same as that of the top angle but formed only in the tension zone.

(6) Based on the yield line theory, design equations were proposed to calculate the characteristic bending capacity of unstiffened, stiffened, and web angle joints. The equations demonstrate predictive capability when directly compared against FEM results across a wide parameter range, showing a consistent and conservative bias without the need for empirical calibration. The calculated values show satisfactory agreement with numerical benchmarks, with errors generally within an acceptable range for practical design.

(7) The design equations and conclusions presented in this study are primarily derived from FEM parametric analyses. While the FEM methodology was carefully validated against physical tests for the core connection mechanics, direct experimental validation of the through-core bolted HSSC angle joint under monotonic and cyclic loading remains an essential next step. Furthermore, the applicability of the yield line patterns and formulas is confined to the parameter ranges investigated. Future work should encompass experimental testing to confirm the predictions, investigation under cyclic loading to evaluate seismic performance metrics, and expansion of the parametric scope to include a wider variety of geometric configurations.

Acknowledgments

The authors wish to acknowledge supports from the Science and Technology Plan Project of Housing and Urban-Rural Development of Shandong Province (2024KYKF-JZGYH101).

References

[1] D.K. Miller. Lessons learned from the Northridge earthquake, Engineering Structures. 20 (1998) 249-260. https://doi.org/10.1016/S0141-0296(97)00031-X.
[2] H. Akiyama. Evaluation of fractural mode of failure in steel structures following Kobe lessons, Journal of Constructional Steel Research. 55 (2000) 211-227. https://doi.org/10.1016/S0143-974X(99)00086-3.
[3] J. Gracia, E. Bayo, F. Ferrario et al. The seismic performance of a semi-rigid composite joint with a double-sided extended end-plate. Part I: Experimental research, Engineering Structures. 32 (2010) 385-396. https://doi.org/10.1016/j.engstruct.2009.10.003.
[4] Z.Y. Kong, S.Z. Hong, Q.V. Vu, et al. New equations for predicting initial stiffness and ultimate moment of flush end-plate connections, Journal of Constructional Steel Research. 175 (2020) 106336. https://doi.org/10.1016/j.jcsr.2020.106336.
[5] G. Shi, X.S. Chen. Moment-rotation curves of ultra-large capacity end-plate joints based on component method, Journal of Constructional Steel Research. 128 (2017) 451-461. https://doi.org/10.1016/j.jcsr.2016.09.012.
[6] P. Wang. Study on Mechanical Behaviors of Beam-to-Column Connection with Stiffened Top and Seat Angles. 2018. [in Chinese]
[7] D.D. Sun, Y. Yang, Y.K. Ma, et al. Seismic performance of resilient beam-column connection using replaceable stiffener angle steel, Journal of Constructional Steel Research. 196 (2022) 107370. https://doi.org/10.1016/j.jcsr.2022.107370.
[8] X.N. Cai, N.N. Gong, C.C. Fu, et al. Seismic behavior of self-centering prestressed precast concrete frame subassembly using steel top and seat angles, Engineering Structures. 229 (2021) 111646. https://doi.org/10.1016/j.engstruct.2020.111646.
[9] D. Skejic, D. Dujmovic, D. Beg. Behaviour of stiffened flange cleat joints, Journal of Constructional Steel Research. 103 (2014) 61-76. https://doi.org/10.1016/j.jcsr.2014.07.011.
[10] EN 1993-1-5:2006. Eurocode 3: Design of steel structures - Part 1-5: General rules - Plated structural elements, European Committer for Standardization. 2004.
[11] J.M. Reinosa, A. Loureiro, R. Gutierrez, et al. Analytical plate approach for the axial stiffness prediction of stiffened angle cleats, Journal of Constructional Steel Research. 106 (2015) 77-88. https://doi.org/10.1016/j.jcsr.2014.12.010.
[12] D. Skejic, D. Dujmovic, M. Rak. Laboratory testing of angle flange cleats in bending, Gradjevinar. 65 (2010) 207-218.
[13] S. Movagati, A.E. Abdelnaby. Experimental study on the nonlinear behavior of bearing-type semi-rigid connections, Engineering Structures. 199 (2019) 109609. https://doi.org/10.1016/j.engstruct.2019.109609.
[14] P. Wang, J.R. Pan, Z. Wang. Experimental and analytical behavior of stiffened angle joints, Steel and Composite Structures. 26 (2018) 67-78. https://doi.org/10.12989/scs.2018.26.1.067.
[15] P. Wang, J.R. Pan, Z. Wang, et al. Experimental and numerical investigation of stiffened angle connection in a minor axis, Science Progress. 103 (2020) 1-27. DOI: 10.1177/0036850420973521.
[16] J. Xu, Z. Wang, P. Wang, et al. Numerical investigations on large size stiffened angle

connections with different bolt patterns, Journal of Constructional Steel Research. 182 (2021) 106670. https://doi.org/10.1016/j.jcsr.2021.106670.
[17] Y. Zhang, S. Gao, E.X. Du, et al. Ultimate tensile properties of bolted stiffened angle connections, Structures. 55 (2023) 2370-2388. https://doi.org/10.1016/j.istruc.2023.07.047.
[18] B. Meng, H. Li, D.Y. Kong, et al. Development of an enhanced top-and seat-angle connection to mitigate progressive collapse, Journal of Constructional Steel Research. 211 (2023) 108116. https://doi.org/10.1016/j.jcsr.2023.108116.
[19] Z.Y. Kong, S.E. Kim. Moment-rotation behavior of top-and seat-angle connections with double web angles, Journal of Constructional Steel Research. 128 (2017) 428-439. https://doi.org/10.1016/j.jcsr.2016.09.010.
[20] J.M. Reinosa, A. Loureiro, R. Gutierrez, et al. Mechanical stiffness prediction of beam-to-column stiffened angle joints, Journal of Constructional Steel Research. 168 (2020) 105875. https://doi.org/10.1016/j.jcsr.2019.105875.
[21] M.J. Hasan, M. Ashraf, B. Uy. Moment-rotation behaviour of top-seat angle bolted connections produced from austenitic stainless steel, Journal of Constructional Steel Research. 136 (2017) 149-161. https://doi.org/10.1016/j.jcsr.2017.05.014.
[22] M.J. Hasan, S. Al-Deen, M. Ashraf. Behaviour of top-seat double web angle connection produced from austenitic stainless steel, Journal of Constructional Steel Research. 155 (2019) 460-479. https://doi.org/10.1016/j.jcsr.2018.12.015.
[23] H. AlHendi, M. Mahmoud, M. Celikag. Numerical study of top-and seat-angle with double web-angle connection with high-strength steel, Journal of Constructional Steel Research. 174 (2020) 106297. https://doi.org/10.1016/j.jcsr.2020.106297.
[24] Y.F. Cao, Y.L. Lu, J. Jiang, et al. Experimental study on behavior of top-and-seat-angle with double web-angle (TSDW) connections under fire conditions, Thin-Walled Structures. 194 (2024) 111304. https://doi.org/10.1016/j.tws.2023.111304.
[25] ABAQUS Analysis user's manual, ABAQUA Standard. 2022.
[26] L.L. Sun, M. Liu, Y.J. Liu, et al. Studies on T-shaped one-side bolted connection to hollow section column under bending, Journal of Constructional Steel Research 175 (2020) 106359. https://doi.org/10.1016/j.jcsr.2020.106359.
[27] G.L. Hou, Y.T. Shang, L. Zhang, et al. Bending performance of bolted beam-column joints with T-stubs, Journal of Constructional Steel Research. 226 (2025) 109280. https://doi.org/10.1016/j.jcsr.2024.109280.
[28] GB 50017-2017. Standard for design of steel structures, China Architecture & Building Press. 2017.
[29] M.S. Zhao, C.K. Lee, S.P. Chiew. Tensile behavior of high performance structural steel T-stub joints, Journal of Constructional Steel Research. 122 (2016) 316-325. https://doi.org/10.1016/j.jcsr.2016.04.001.
[30] A. Loureiro, A. Moreno, R. Gutiérrez, et al. Experimental and numerical analysis of three-dimensional semi-rigid steel joints under non-proportional loading, Engineering Structures. 38 (2012) 68-77. https://doi.org/10.1016/j.engstruct.2011.12.048.
[31] J.M. Cabrero, E. Bayo. The semi-rigid behaviour of three-dimensional steel beam-to-column joints subjected to proportional loading. Part I. Experimental evaluation, Journal of Constructional Steel Research. 63 (2007) 1241-1253. https://doi.org/10.1016/j.jcsr.2006.11.004.
[32] M.M. Tahir, H. Mohammadhosseini, S.P. Ngian, et al. I-beam to square hollow column blind bolted moment connection: Experimental and numerical study, Journal of Constructional Steel Research. 148 (2018) 383-398. https://doi.org/10.1016/j.jcsr.2018.06.012.
[33] P.J. Wang, L.L. Sun, B.X. Zhang, et al. Experimental studies on T-stub to hollow section column connection bolted by T-head square-neck one-side bolts under tension, Journal of Constructional Steel Research. 178 (2021) 106493. https://doi.org/10.1016/j.jcsr.2020.106493.
[34] GB/T 706-2016. Hot rolled section steel, Standards Press of China. 2016.
[35] GB/T 19879-2023. Steel plate for building structure, Standards Press of China. 2023.
[36] Publication Number: P398. Joints in Steel Construction: Moment-Resisting Joints to Eurocode 3, The Steel Construction Institute. 2013.
[37] EN 1993-1-8:2005. Eurocode 3: Design of steel structures - Part 1-8: Design of joints, European Committer for Standardization. 2005.